SEASONAL VARIABILITY OF MODE-1 AND MODE-2 INTERNAL SOLITARY WAVES OFF THE AMAZON SHELF OBSERVED FROM MODIS/TERRA SUNGLINT IMAGES.

Carina Regina de Macedo[1,2], Ariane Koch-Larrouy[2], José Carlos B. da Silva[3] Carlos Alessandre D. Lentini[4], Jorge Manuel Magalhães[3], Trung Kien Tran[1], Marcelo Caetano B. Rosa[4] and Vincent Vantrepotte[1]

[1]Univ. Lille, CNRS, Univ. Littoral Côte d'Opale, UMR 8187 - LOG - Laboratoire d'Océanologie et de Géosciences, F-59000 Lille, France, Email:carina.macedo@fc.up.pt, trung-kien.tran@univ-littoral.fr, vincent.vantrepotte@univ-littoral.fr, [2]LEGOS, Université de Toulouse, CNES, CNRS, IRD, UPS, Toulouse, France, Ariane.koch-larrouy@legos.obs-mip.fr; [3]Department of Geosciences, Environment and Spatial Planning, Faculdade de Ciências da Universidade do Porto, Porto, Portugal, Email: jdasilva@fc.up.pt, jmagalhaes@fc.ul.pt and [4]Universidade Federal da Bahia – IF/UFBA, Salvador, Brazil, Email:clentini@ufba.br, marcelorosa2005@yahoo.com.br

ABSTRACT

This study focuses on the Amazon ISWs occurrence, their velocity/wavelength, and variability at seasonal cycles. The analysis is based on a data set composed of 71 MODIS/TERRA images, where more than 250 internal solitary wave (ISW) signatures were identified in the sun glint area. ISWs packets separated by typical mode-1 and mode-2 internal tides (ITs) wavelengths have been identified and mapped coming from sites A, and B. In area B, the mode-1 and mode-2 ISWs seem to have lower wavelengths than the ones in area A. Mode-1 ISWs from site A showed higher wave velocity/wavelength during the boreal summer/fall, with higher diversity in terms of propagation velocities. Calculations of the IT velocities using the Taylor-Goldstein equation supported our results of shorter-scale ISWs associated with mode-2 IT wavelengths in the study area and additionally into the ISW/IT seasonal variability.

Key words – *Internal Solitary waves, Internal tides, MODIS/TERRA, Amazon shelf, seasonal variability.*

1. INTRODUCTION

The Amazon shelf is an important hotspot for intense internal tides (IT) and internal solitary waves (ISWs) generation. ISWs propagating offshore are associated with the disintegration of IT several hundred kilometers from their generation sites over the steep slopes of the Amazon shelf break [1]. More than 6 sites of IT generation were identified, the sites called A and B are the strongest [1, 2].

Seasonal variability of the circulation and stratification is linked to changes in the IT and ISW propagation direction, intensity, wavelength, and velocity [1, 2]. During the boreal summer/fall, the North Equatorial Countercurrent (NECC) enhances the ISWs velocity and refracts them toward the northeast [1]. Changes in the IT baroclinic mode and wavelength were linked to the seasonality of the pycnocline depth and its strength in the Amazon shelf [3, 2]. The mode-2 ITs are impacted by the water stratification associated with seasonal variability in the Amazon basin [3, 2]. During the boreal spring, the shallower and slightly strong pycnocline enhances the generation of higher baroclinic modes ITs, enhancing the local dissipation [2].

In the study area, ISWs with an average inter-packet distance with typical wavelengths of long (semi-diurnal) ITs of the fundamental mode (i.e., mode-1 ITs) were studied by [1]. However, the signatures of small-scale ISWs with average inter-packet distance with a typical wavelength of mode-2 ITs trailing larger ISWs was briefly reported by [4]. Signatures of small-scale ISWs trailing larger ISWs have been documented in the South China Sea, Mascarene Ridge of the Indian Ocean, and Andaman Sea [5, 6, 7].

Remote sensing (RS) provides new insights into the ISW generation, propagation, and dissipation mechanisms. Signatures of ISWs on sun glint imagery are produced by variations of short-scale sea surface roughness which cause changes in the image glitter brightness [8, 9]. Since ISWs produce leading bands of rough followed by smooth sea surface roughness associated, respectively, with convergent and divergent surface currents, this oceanic feature can be observed in sun glint imagery [10, 8].

This study focus on the use of a comprehensive data set of Moderate Resolution Imaging Spectroradiometer (MODIS) images onboard the TERRA satellite from Jan-2005 to Dec-2013 to study the ISWs off the Amazon shelf. ISWs with inter-packet distance with typical wavelengths of mode-1 ITs and wave tails (small-scale ISWs with inter-packet distance with typical wavelengths of mode-2 ITs) have been mapped and their propagation velocities are analyzed, considering their seasonal variability. The presence of shorter-scale ISWs tails separated by mode-2 IT wavelengths and the ISW/IT seasonal variability was supported by calculations of the IT phase velocities using the Taylor-Goldstein equation (TGE).

2. MATERIAL AND METHODS

The RS data set is composed of 71 Level 1B MODIS/TERRA images from 01 January 2005 to 31 December 2013 acquired off the Amazon shelf (https://earthdata.nasa.gov/). The Global Ocean Ensemble Physics Reanalysis (EPR) data provides a 3D-gridded description of the global oceanic physical state at 0.25-degree resolution (https://marine.copernicus.eu/). The product is a multi-numerical ocean model ensemble approach and data assimilation of satellite and *in situ* observations. The daily mean average of temperature, salinity, and currents variables was acquired from 2005 to 2013 for 75 vertical levels.

The ISW signatures were visually identified and manually extracted in the sun glint region. The distance of the vector

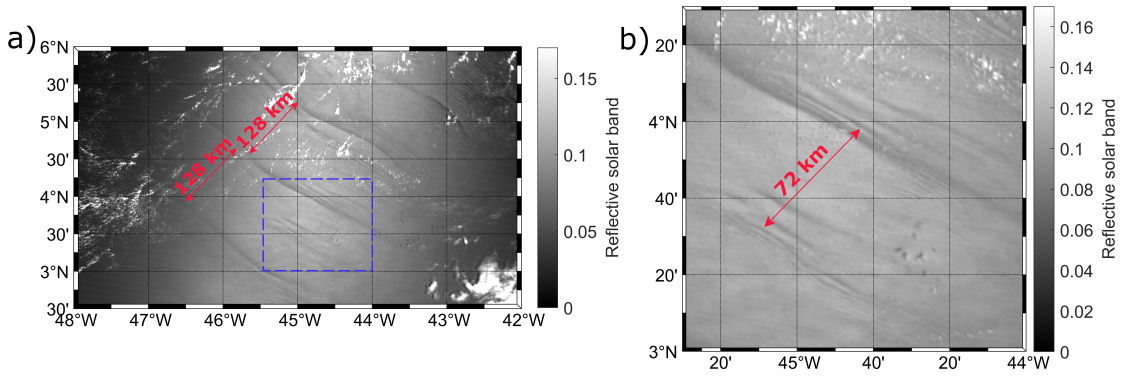

Figure 1: Level 1B MODIS/TERRA image, band 6, acquired on 10th October 2014 shows: (a) a typical view of this study region in which it can be seen that ISW signatures are often found with mode-1 and mode-2 IT wavelengths. The blue rectangle represents the area where (b) signatures associated with mode-2 ITs are found.

which connects the middle point of each consecutive leading wave of each ISW packet was calculated, perpendicular to the ISW crests which we call inter-packet distance or wavelength since it is associated with typical IT wavelengths. The average wave propagation velocity was calculated considering the period of the semi-diurnal IT of 12.42 hours. The study region is presented in Figure 1, where ISW signatures with typical mode-1 and mode-2 IT wavelengths (hereafter called mode-1 and mode-2 ISWs) are present. The ISW propagation direction, pd, was automatically retrieved from the RS data considering the angle between the North and the direction of the vector which connects the middle point of two consecutive packets (in a clockwise direction), i. e., $pd = 0°$ means ISWs propagating from the South to the North and $pd = 90°$ means propagating from West to East.

The waves' velocities of all modes are predicted using the viscous TGE [11, 12]:

$$\sigma \begin{pmatrix} \nabla^2 & \mathbf{0} \\ \mathbf{0} & \mathbf{I} \end{pmatrix} \begin{pmatrix} \hat{w} \\ \hat{b} \end{pmatrix} = \begin{pmatrix} -ikU\nabla^2 + ik\frac{d^2U}{dz^2} + T_w & -k^2 \\ -\frac{dB}{dz} & -ikU + T_b \end{pmatrix} \begin{pmatrix} \hat{w} \\ \hat{b} \end{pmatrix} \quad (1)$$

where $\mathbf{0}$ and $\mathbf{I}$ are the zero and identity matrices, respectively. The complex vertical structure functions of vertical buoyancy and velocity are, respectively, $\hat{b}$ and $\hat{w}$. $k = \sqrt{k_z^2 + k_m^2}$ is the wave number magnitude, with k_z and k_m being a real wave number with zonal and meridional components. U is the shear flow. T_w and T_b are the viscous and diffusive operators. Considering, $\nabla^2 = d^2/dz^2 - k^2$, the boundary conditions is $\hat{w} = 0$ (impermeable) and $\hat{b} = 0$ (constant buoyancy).

The local values of stratification and shear were taken from monthly reanalysis data for each location where ISWs were identified. The current velocities were decomposed in the ISW traveling direction, where positive velocity means current flowing in the same direction as the ISWs/IT; while a negative one means current flowing in the opposite direction. The separation between the different wave modes is based on the probability distribution of the velocities predicted by the viscous TGE for mode-1 and mode-2 ITs, considering the monthly reanalysis data.

3. RESULTS

In total, 250 ISW signatures were identified in the study area, where 206 correspond to mode-1 and 47 to mode-2 waves (respectively, Figure 2-(a) and (b)). The ISW signatures detected by visual analysis emanate from several IT generation sites mainly from A, and B as previously described by [1, 2]. The average wavelength and velocity of ISW calculated from RS data are presented in Table 1 and the results for areas A and B are shown in boxplot format in Figure 2-(a) and (b), respectively. In area A, a total of 233 signatures were identified, 18% mode-2 waves; while in area B 17 signatures were mapped with mode-2 waves being 29%. In the area, A and B, [1] observed ISWs of fundamental mode propagating with similar mean velocities (i. e., respectively, 3.1 m.s^{-1} and 2.7 m.s^{-1}). In area B, the mode-1 and mode-2 wavelength is about, respectively, 9% and 3% lower than the wavelength of the waves in area A.

For area A, the seasonal variability of the ISW characteristics in terms of velocity and wavelength has been characterized considering the two well-marked seasons on the Amazon shelf, i. e. the boreal spring (from March to July) and the boreal summer/fall (from August to December) following [2]. The analysis was not performed for area B because of the lack of measurements during the boreal spring. Figure 4-(a) and (b) shows the results in boxplot format for, respectively, mode-1 and mode-2 waves. A marked difference between spring and summer/fall is found for mode-1 waves, with the mean ISW wavelength being 15% lower during spring (see Table 2). Larger ISW wavelengths during the boreal summer/fall can be linked to the deeper pycnocline and the stronger currents linked to the reinforcement of the North Equatorial Countercurrent in the study area when compared to spring period [3, 2, 1]. Furthermore, during the boreal summer/fall, the waves are characterized by a higher diversity in terms of their wavelengths (higher standard deviation), suggesting a higher variability of the local stratification and current shear patterns in the study area during that season. In [1], the author found an increase of 30% in the mode-1 ISWs velocities during the boreal summer/fall based on the study of two showcases (one of them from May and the other one from October). For mode-2 waves, the differences between the two seasons are less evident, with the mean ISW

Area	Baroclinic mode	Data Source	Wavelength (km) (mean ± std)	Velocity (m.s^{-1}) (mean ± std)
A	Mode-1	RS	134.6 ± 15.7	3.0 ± 0.4
		TGE	109.2 ± 8.4	2.4 ± 0.19
	Mode-2	RS	69.8 ± 7.4	1.7 ± 0.2
		TGE	70.4 ± 4.8	1.6 ± 0.1
B	Mode-1	RS	122.5 ± 16.4	2.7 ± 0.4
		TGE	104.7 ± 4.7	2.3 ± 0.1
	Mode-2	RS	67.5 ± 14.9	1.5 ± 0.3
		TGE	67.1 ± 4.6	1.5 ± 0.1

Table 1: Average wavelength and velocity of mode-1 and mode-2 ISW calculated from RS data and of IT predicted by solving the TGE for both areas A and B.

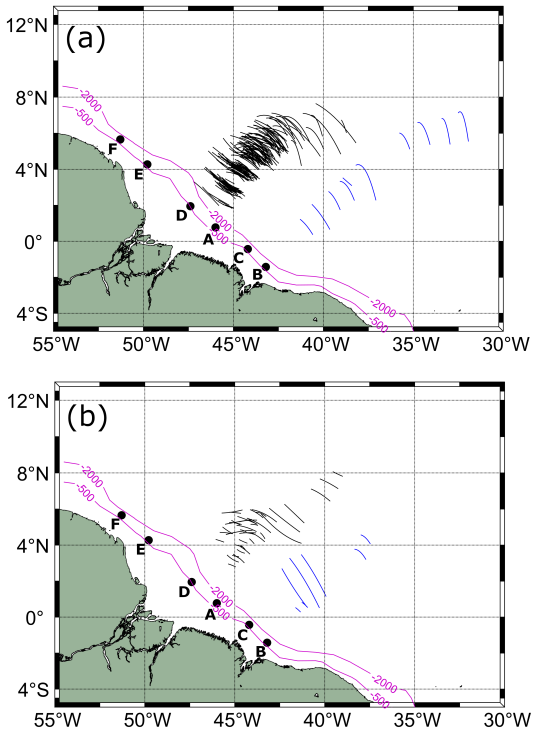

Figure 2: (a) mode-1 and (b) mode 2 ISW composite map derived from 71 MODIS/TERRA data acquired under sun glint conditions from 2005 to 2013. Black, and blue solid lines correspond to ISW signatures which emanate likely from IT generation points A, and B, respectively.

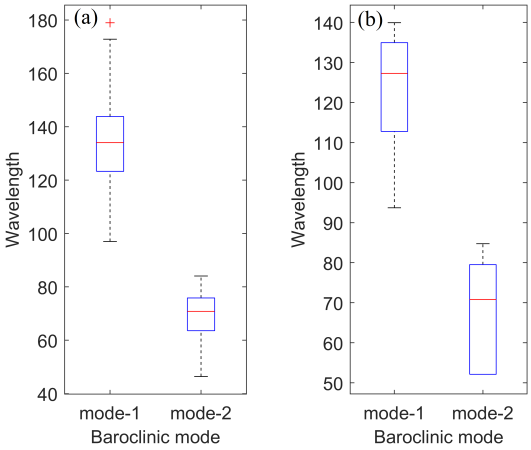

Figure 3: Mode-1 and mode-2 ISW wavelengths organized in boxplot format for (a) area A, and (b) area B.

wavelength during the boreal spring being 5% lower than during the summer/fall. It is important to point out that during the boreal spring we have few samples of mode-2 waves, which can compromise our results.

4. DISCUSSION

The calculated IT wavelengths/velocities by mode-1 and mode-2 waves in areas A and B using the TGE varies in a similar pattern which was found in the analysis of the ISW from the RS scenes (see Table 1), supporting our decision to split the waves into two different baroclinic modes. The calculated mode-1 mean wavelength/velocity is underestimated by about 19% and 15%, respectively, for areas A and B. In [13], the authors found an underestimation of the phase speed calculated by the TGE of about 12% in the Mascarene Plateau. The nonlinear phase speed is positively proportional to the surface wave elevation [14, 3, 2], which explains the higher differences between the mode-1 wavelengths/velocities calculated from the TGE and estimated from the RS scenes when compared to the mode-2 waves, which have a good agreement with the simulated data. In [2], the authors have separated mode-1 and mode-2 IT off the Amazon shelf considering, respectively, the wavelength bands of 100-150 km and 50-75 km, which are in fair agreement with our calculations.

The simulated results using the TGE could reproduce quite well the differences between the two seasons, with the predicted mode-1 and mode-2 wavelengths during the boreal spring being, respectively, about 9.5% and 7.7% lower than during the summer/fall. Although the differences in the mode-1 propagation velocities/wavelength between ASOND and MAMJJ are underestimated by the theoretical method, the TGE results gave us important insights to support our analysis principally considering our unbalanced data set according to the seasons.

5. CONCLUSIONS

The conclusions are summarized as follows:

- The ISW signatures detected from RS scenes emanate from mainly IT generation sites A and B.
- In area B the mode-1 and mode-2 ISWs seem to have lower wavelengths than the ones in area A.
- A marked difference between spring and summer/fall is found for mode-1 waves in area A, with the mean ISW

Baroclinic mode	Season	Data Source	Wavelength (km) (mean ± std)	Velocity (m.s^{-1}) (mean ± std)
Mode-1	Spring	RS	116.7 ± 5.7	2.6 ± 0.1
		TGE	104.6 ± 5.6	2.3 ± 0.1
	Summer/fall	RS	137.7 ± 15.0	3.1 ± 0.3
		TGE	115.6 ± 10.6	2.6 ± 0.2
Mode-2	Spring	RS	66.5 ± 11.8	1.5 ± 0.3
		TGE	67.9 ± 4.0	1.5 ± 0.1
	Summer/fall	RS	70.4 ± 6.6	1.6 ± 0.1
		TGE	73.6 ± 5.3	1.6 ± 0.1

Table 2: Average wavelength and velocity of mode-1 and mode-2 ISW calculated from RS data and of IT predicted by solving the TGE according to two seasons in area A.

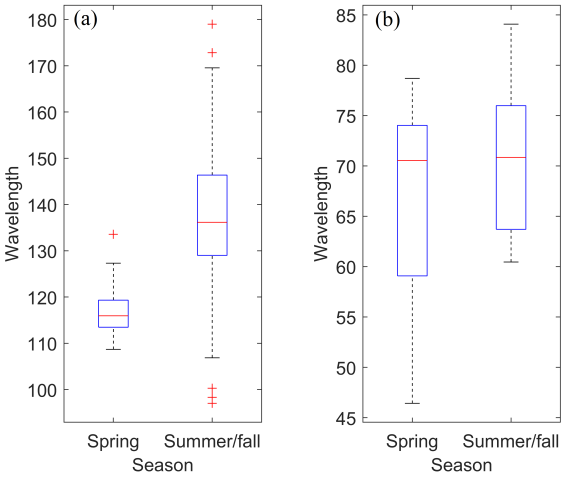

Figure 4: Seasonal variability of the ISW wavelengths organized in boxplot format for (a) mode-1 and (b) mode-2 waves in area A.

wavelength being 15% lower during spring.

- The mode-1 ISWs are characterized by a higher diversity in terms of their wavelengths during the boreal summer/fall.
- For mode-2 waves, the differences between the two seasons are less evident, with the mean ISW wavelength in spring being 5% lower than during the summer/fall.
- The calculated IT wavelengths/velocities by mode-1 and mode-2 waves in areas A and B using the TGE vary in a similar pattern which was found in the analysis of the ISW from the RS scenes.
- The simulated results using the TGE could reproduce quite well the differences between the boreal spring and summer/fall.

6. REFERENCES

[1] JM Magalhães, JCB da Silva, MC Buijsman, and CAE Garcia. Effect of the north equatorial counter current on the generation and propagation of internal solitary waves off the amazon shelf (sar observations). *Ocean Science*, 12(1):243–255, 2016.

[2] M Tchilibou, A Koch-Larrouy, S Barbot, F Lyard, Y Morel, J Jouanno, and R Morrow. Internal tides off the amazon shelf during two contrasted seasons: Interactions with background circulation and ssh imprints. *Ocean Science Discussions*, pages 1–38, 2022.

[3] S Barbot, F Lyard, M Tchilibou, and L Carrere. Background stratification impacts on internal tide generation and abyssal propagation in the western equatorial atlantic and the bay of biscay. *Ocean Science*, 17(6):1563–1583, 2021.

[4] JCB da Silva, JM Magalhães, MC Buijsman, and CAE Garcia. Sar imaging of wave tails: Recognition of second mode internal wave patterns and some mechanisms of their formation. *Living Plannet Symposium 2016*, 2016.

[5] C Guo, V Vlasenko, W Alpers, N Stashchuk, and X Chen. Evidence of short internal waves trailing strong internal solitary waves in the northern south china sea from synthetic aperture radar observations. *Remote Sensing of Environment*, 124:542–550, 2012.

[6] JCB da Silva, MC Buijsman, and JM Magalhães. Internal waves on the upstream side of a large sill of the mascarene ridge: A comprehensive view of their generation mechanisms and evolution. *Deep Sea Research Part I: Oceanographic Research Papers*, 99:87–104, 2015.

[7] JM Magalhães and JCB Da Silva. Internal solitary waves in the andaman sea: New insights from sar imagery. *Remote Sensing*, 10(6):861, 2018.

[8] CR Jackson and W Alpers. The role of the critical angle in brightness reversals on sunglint images of the sea surface. *Journal of Geophysical Research: Oceans*, 115(C9), 2010.

[9] V Kudryavtsev, A Myasoedov, B Chapron, JA Johannessen, and F Collard. Joint sun-glitter and radar imagery of surface slicks. *Remote sensing of environment*, 120:123–132, 2012.

[10] W Alpers. Theory of radar imaging of internal waves. *Nature*, 314(6008):245–247, 1985.

[11] WD Smyth, JN Moum, and JD Nash. Narrowband oscillations in the upper equatorial ocean. part ii: Properties of shear instabilities. *Journal of Physical Oceanography*, 41(3):412–428, 2011.

[12] Q Lian, WD Smyth, and Z Liu. Numerical computation of instabilities and internal waves from in situ measurements via the viscous taylor–goldstein problem. *Journal of Atmospheric and Oceanic Technology*, 37(5):759–776, 2020.

[13] JCB da Silva, AL New, and JM Magalhães. On the structure and propagation of internal solitary waves generated at the mascarene plateau in the indian ocean. *Deep Sea Research Part I: Oceanographic Research Papers*, 58(3):229–240, 2011.

[14] DRG Jeans. Solitary internal waves in the ocean: A literature review completed as part of the internal wave contribution to morena. uces. *Marine Science Labs, University of North Wales. Rep. U-95*, 1995.